# THE UNEXPECTED KINEMATICS OF MULTIPLE POPULATIONS IN NGC 6362: DO BINARIES PLAY A ROLE?[*]

E. Dalessandro,[1] A. Mucciarelli,[2, 1] M. Bellazzini,[1] A. Sollima,[1] E. Vesperini,[3] J. Hong,[3, 4] V. Hénault-Brunet,[5] F.R. Ferraro,[2, 1] R. Ibata,[6] B. Lanzoni,[2, 1] D. Massari,[7] and M. Salaris[8]

[1] *INAF-Astrophysics and Space Science Observatory, Via Gobetti 93/3 40129 Bologna - Italy*
[2] *Dipartimento di Fisica & Astronomia, Universitá degli Studi di Bologna, Via Gobetti 93/2 40129 Bologna - Italy*
[3] *Department of Astronomy, Indiana University, Swain West, 727 E. 3rd Street, IN 47405 Bloomington - USA*
[4] *Kavli Institute for Astronomy and Astrophysics, Peking University, Yi He Yuan Lu 5, HaiDian District, Beijing 100871, China*
[5] *National Research Council, Herzberg Astronomy & Astrophysics, 5071 West Saanich Road, Victoria, BC, V9E 2E7, Canada*
[6] *Observatoire Astronomique, Université de Strasbourg, CNRS, 11 rue de l'Université, F-67000 Strasbourg, France*
[7] *Kapteyn Astronomical Institute, University of Groningen, Groningen, The Netherlands Leiden Observatory, Leiden University, Leiden, The Netherlands*
[8] *Astrophysics Research Institute, Liverpool John Moores University, IC2 Liverpool Sceince Park, 146 Brownlow Hill, L3 5RF, Liverpool*

## ABSTRACT

We present a detailed analysis of the kinematic properties of the multiple populations (MPs) in the low-mass Galactic globular cluster NGC 6362 based on a sample of about 500 member stars for which radial velocities (RVs), Fe and Na abundances have been homogeneously derived.

At distances from the cluster center larger than about $0.5r_h$, we find that first (FG - Na-poor) and second generation (SG - Na-rich) stars show hints of different line-of-sight velocity dispersion profiles, with FG stars being dynamically hotter. This is the first time that differences in the velocity dispersion of MPs are detected by using only RVs. While kinematic differences between MPs in globular clusters are usually described in terms of anisotropy differences driven by the different radial distributions, this explanation seems hardly viable for NGC 6362, where SG and FG stars are spatially mixed. We demonstrate that the observed difference in the velocity dispersion profiles can be accounted for by the effect of binary stars. In fact, thanks to our multi-epoch RV measurements we find that the binary fraction is significantly larger in the FG sample ($f \sim 14\%$) than in SG population ($f < 1\%$), and we show that such a difference can inflate the velocity dispersion of FG with respect to SG by the observed amount in the relevant radial range. Our results nicely match the predictions of state-of-the art $N$-body simulations of the co-evolution of MPs in globular clusters that include the effect of binaries.

Corresponding author: Emanuele Dalessandro
emanuele.dalessandro@oabo.inaf.it

# 1. INTRODUCTION

The discovery of multiple populations (MPs) in globular clusters (GCs), differing in light-elements abundance (e.g. He, C, N, O, Na, Mg, Al) while having the same iron (and iron-peak elements) content, has seriously challenged our understanding of the physical mechanisms driving the formation and early evolution of these systems (see Gratton et al. 2012; Bastian & Lardo 2017 for a review). Indeed it is now well established that almost all relatively massive ($\sim 10^4 M_\odot$; e.g. Piotto et al. 2015; Bragaglia et al. 2017) and old ($> 2$ Gyr; see for example Martocchia et al. 2017) GCs host MPs.

Spectroscopically MPs manifest themselves in the form of light-element anti-correlations (like C-N, Na-O, Mg-Al). These chemical inhomogeneities produce also a variety of features in the color-magnitude diagrams (CMDs) when appropriate near-UV bands are used (Sbordone et al. 2011). Thanks to spectro-photometric studies, MPs have been directly observed in many GCs in the Galaxy (see Piotto et al. 2015 for a recent homogeneous collection) as well as in external systems (like the Magellanic Clouds and the Fornax dwarf galaxy - Mucciarelli et al. 2009; Dalessandro et al. 2016; Larsen et al. 2014). Moreover, the presence of MPs has been indirectly constrained in the GC systems of M31 and M87 (Schiavon et al. 2013; Chung et al. 2011).

Different scenarios have been proposed over the years to explain the formation of MPs. They generally invoke a self-enrichment process, which likely occurred in the very early epochs of GC formation and evolution. In these scenarios, it is thought that a second generation/population (SG) formed from the ejecta of stars (polluters) to a first generation/population (FG) mixed with "pristine material" (Decressin et al. 2007; D'Ercole et al. 2008; de Mink et al. 2009; Bastian et al. 2013; Denissenkov & Hartwick 2014). However, all models proposed so far face serious problems and a self-consistent explanation of the physical processes at the basis of MP formation is still lacking.

Understanding the kinematical properties of MPs can provide new important insights on GC formation and evolution. One of the predictions of MP formation models (e.g. D'Ercole et al. 2010) is that SG stars form a low-mass and centrally segregated stellar sub-system possibly characterized by a more rapid internal rotation than the (more spatially extended) FG system (Bekki 2010). Although the long-term dynamical evolution of stars can smooth out the initial structural and kinematical differences between FG and SG to a large extent, some are expected to be still visible in present-day GCs (see for example Vesperini et al. 2013; Hénault-Brunet et al. 2015). First evidence of the difference in the structural properties of MPs were based on their spatial distributions (Lardo et al. 2011; Milone et al. 2012; Bellini et al. 2013; Dalessandro et al. 2016; Massari et al. 2016). These works have shown that indeed SGs are typically more centrally concentrated than FG sub-populations, with few remarkable exceptions (see Dalessandro et al. 2014; Larsen et al. 2015; Savino et al. 2018). However, spatial distributions alone provide only a partial picture of the dynamical properties of MPs and key constraints on the possible formation and dynamical paths of MPs may be hidden in their kinematic properties.

Hints of different degrees of orbital anisotropy among MPs have been found in the massive GCs 47 Tuc and NGC 2808 by means of HST proper motions (Richer et al. 2013; Bellini et al. 2015). These findings seem to be consistent with the kinematical fingerprints of the diffusion of the SG population from the innermost regions towards the cluster outer zones and provide indirect support to formation scenarios predicting SG formed in a centrally concentrated subsystem.

Cordero et al. (2017) found also that the extremely enriched component of SG stars in M 13 shows a larger rotation amplitude than other stars in the cluster.

In general, however, MP kinematics is still poorly constrained, mainly because of technical limitations related to the difficulty of deriving kinematical information in dense environments for large and significant samples of resolved stars adequately separated in terms of their light elements abundances.

Here we present the results of an extended kinematical analysis of the MPs in the Galactic GC NGC 6362, based on the radial velocities (RVs) of a large sample ($\sim$ 800) of stars chemically tagged according to the sub-population they belong to. The case of NGC 6362 is particularly interesting. Indeed, this is possibly the second least massive ($M \sim 5 \times 10^4 M_{\odot}$) GC[1] where MPs have been identified both photometrically and spectroscopically (Dalessandro et al. 2014; Mucciarelli et al. 2016) so far. Also, contrary to what is generally observed in other GCs (see, e.g., Lardo et al. 2011), we have found that in this cluster the spatial distributions of MPs are consistent with complete mixing over the entire cluster extension (Dalessandro et al. 2014). This behavior suggests that the cluster underwent complete spatial redistribution of stars and severe mass-loss due to long-term dynamical evolution (Vesperini et al. 2013; Dalessandro et al. 2014; Miholics et al. 2015).

The paper is structured as follows. In Section 2, the data-base and data-reduction are presented, in Section 3 sample selection criteria are described, while in Section 4 we report on the main results of the kinematic analysis. In Section 5 sub-population binary fractions are derived and their impact is estimated by means of an analytic approach. In Section 6 observations are compared to $N$-body models following the evolution of MPs. Conclusions and discussion are presented in Section 7.

## 2. OBSERVATIONS AND DATA-ANALYSIS

### 2.1. *Radial velocities and chemical abundances*

The dataset used in this work consists of spectra obtained using the multi-object facility FLAMES@ESO-VLT (Pasquini et al. 2000) in the UVES+GIRAFFE combined mode and secured in two observing runs. In the first run (Prop. ID: 093.D-0618, PI: Dalessandro) stars have been observed using the GIRAFFE setups HR11 and HR13, sampling the two Na doublets at 5682-5688 $\mathring{A}$ and 6154-6160 $\mathring{A}$. In the second run (Prop. ID: 097.D-0325, PI: Dalessandro), which was devoted to enlarge the sample of available RVs and [Na/Fe] abundances toward fainter magnitudes, we adopted the GIRAFFE setup HR12, in order to cover the Na doublet at 5895-5890 $\mathring{A}$ that is strong enough to be easily measured also at low Signal-to-Noise ratio (SNR). All the UVES targets of both runs have been observed with the UVES Red Arm CD#3 580 set-up. Only red giant branch (RGB) stars brighter than $V \sim 17.6$ and red horizontal branch (RHB) stars have been selected by using the optical and ultraviolet ground-based photometry by Dalessandro et al. (2014). 219 stars were observed with the first run and 585 with the second one, 84 of them are in common between the two runs, thus yielding a total of 720 observed stars in the two observing programs. Many stars in the final sample have been observed up to six times. All the spectra have been reduced with the dedicated ESO pipelines. Some results obtained with the first run have been presented in Mucciarelli et al. (2016) and Massari et al. (2017).

RVs have been measured for each individual spectrum with the code `DAOSPEC` (Stetson & Pancino 2008) using tens of metallic lines. Heliocentric corrections have been applied to each exposure, then the spectra of each target have been co-added together and used for the chemical analysis. In the analysis presented below we adopt for each star the RV estimate obtained from the spectrum with

---

[1] after NGC 6535 which has $M \sim 2 \times 10^4 M_{\odot}$; Piotto et al. 2015; Bragaglia et al. 2017
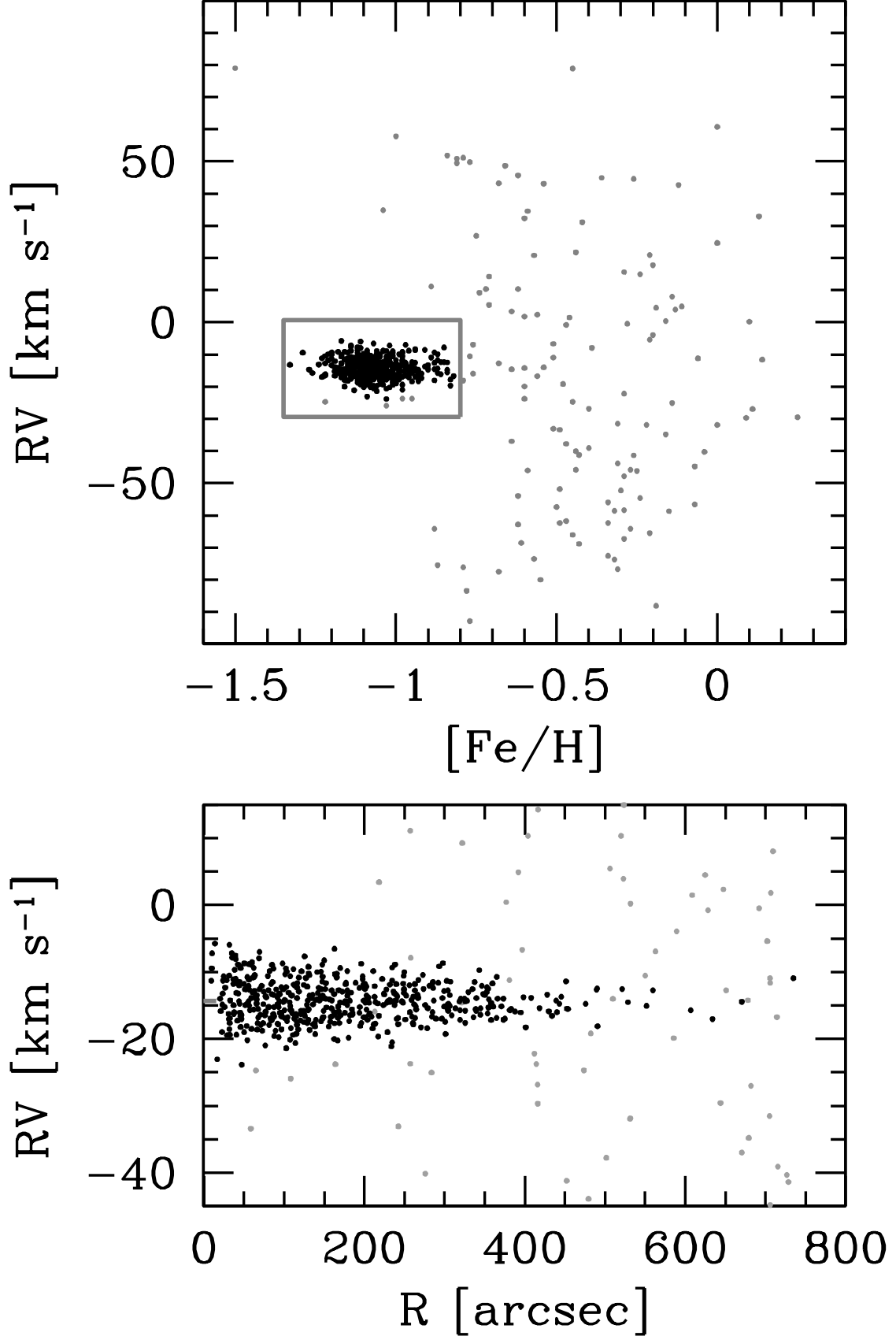
**Figure 1.** Distribution the RVs of the stars in our sample as a function of the derived [Fe/H] (upper panel) and projected distance from the cluster center (bottom panel). Black dots represent stars selected as described in Section 3 and used for the kinematic analysis.
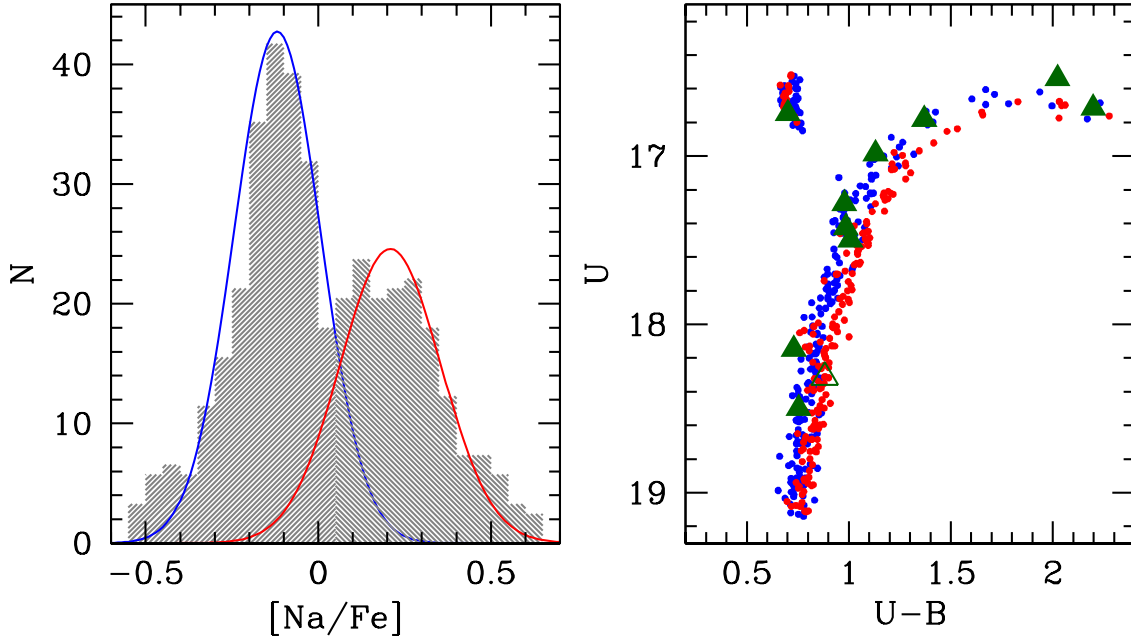
**Figure 2.** *Left panel*: Distribution of the [Na/Fe] abundances of the 489 selected stars. *Right panel*: (U,U-B) CMD of the selected samples (photometry from Dalessandro et al. 2014); *Na-rich* stars are in red and *Na-poor* ones are in blue. Filled green triangles are *Na-poor* binary stars directly detected as described in Section 5, the open triangle is a *Na-rich* binary.

the highest SNR. This allows us to incorporate homogeneously into the final sample the large number of stars having just one spectrum (156) with those having two or more spectra.

Comparing the distribution of the standard deviations ($\sigma_{RV}$) as a function of magnitude, for the stars having at least four independent $RV$ estimates with the distribution of errors on individual best-SNR measures ($\epsilon_{RV}$, as derived by `DAOSPEC`), we noted that, at any given magnitude, $\epsilon_{RV}$ was systematically smaller than $\sigma_{RV}$ (see Kirby et al. 2015). We found that multiplying $\epsilon_{RV}$ by 2 lead to a nearly perfect coincidence of the two distributions, hence we decided to apply this rescaling to get more reliable values of $\epsilon_{RV}$. These rescaled velocity errors have typical values of $\simeq 0.3$ km s$^{-1}$ for $V \leq 15.0$, $\simeq 0.8$ km s$^{-1}$ for $15.0 < V \leq 17.0$, and $\simeq 1.2$ km s$^{-1}$ for $V > 17.0$.

Stellar atmospheric parameters have been determined as in Mucciarelli et al. (2016). Briefly, effective temperatures and surface gravities have been derived from the available photometry; microturbolent velocities have been obtained spectroscopically.

We derived Fe abundances from the measured equivalent widths of $\sim$20-30 (for RGB stars) and $\sim$7-10 (for HB stars) unblended neutral lines using the code `GALA` (Mucciarelli et al. 2013a).

Na abundances have been obtained by fitting the observed lines with a grid of synthetic spectra, in order to take into account the damped wings of the available Na lines. The [Na/Fe] abundances have been corrected for departures from local thermodynamical equilibrium according to Lind et al. (2011). For the sake of consistency we applied the same corrections also to the Na abundances derived in Mucciarelli et al. (2016). Since the [Na/Fe] abundances of the two datasets are based on different Na lines some differences in the resulting abundances might be expected. By using stars in common between the two data-sets we derived an average shift of $(+0.08 \pm 0.01)$dex, which was added before combining all the available measures.

Uncertainties in the abundance ratios have been computed according to the procedure described in Mucciarelli et al. (2013b), which includes both the errors related to the measure of EWs and those arising from the atmospheric parameters.

## 3. SAMPLE SELECTION

Since our main goal is to compare the kinematic properties of FG and SG stars we adopted rather strict selection criteria to avoid contamination from spurious signals of any origin. For this reason we excluded from the final sample all the stars *(a)* lacking reliable Na abundance estimates (mainly due to low SNR or defects in the spectra), *(b)* with $\epsilon_{RV}$ anomalously large for their magnitude, namely $\epsilon_{RV} > 0.8$ km s$^{-1}$ for V$\leq$ 14.9, $\epsilon_{RV} > 1.8$ km s$^{-1}$ for 14.9 <V$\leq$ 16.8, and $\epsilon_{RV} > 2.8$ km s$^{-1}$ for V> 16.8, and *(c)* having $\sigma_{RV} > 3.0$ km s$^{-1}$, as they are likely binary stars with large velocity amplitude.

Figure 1 shows the distribution of RVs as a function of [Fe/H] and as a function of the projected distance from the cluster center (R) for the 632 stars that survived the above selection. Stars belonging to NGC 6362 are easily identified in the *RV*-[Fe/H] diagram as they stand out from the field population at $\sim -15$ km s$^{-1}$ and [Fe/H]$\sim -1.1$. We selected as cluster members the stars within the dark grey box shown in Figure 1 (upper panel), enclosing stars with $-29.3$ km s$^{-1}\leq RV \leq +0.7$ km s$^{-1}$ and $-1.35 <$[Fe/H]$< -0.8$. Finally, studying the velocity distribution of member stars as a function of R, we identified four stars whose *RV* deviates from the systemic velocity of the cluster by more than three times the local value of the velocity dispersion, i.e. the velocity dispersion in a small radial range about their position. Using these selection criteria, we selected a total of 489 bona fide member stars, which we define here as the *total sample*, plotted as black dots in Figure 1. Applying the maximum likelihood (ML) algorithm described in Mucciarelli et al. (2012) to the set of 489 individual [Fe/H] estimate and errors we find $\langle[Fe/H]\rangle = -1.063\pm0.004$ and $\sigma_{[Fe/H]} = 0.000\pm0.006$, in agreement with Mucciarelli et al. (2016). It is reassuring that the outcome of our selection is a sample drawn from a pure single-metallicity population, thus very likely composed only by genuine cluster members.

The Na abundance distribution of member stars (Figure 2 panel a)) is clearly bimodal. This is in agreement with Mucciarelli et al. (2016) based on the much smaller sample (160 member stars) from the first observing run. Using the Gaussian mixture modeling algorithm described by Muratov & Gnedin (2010) we find that the hypothesis of unimodal distribution can be rejected with a probability > 99.9%. Based on the shape of the distribution shown in Figure 2 (panel a)) we define two sub-populations. The first, here defined as *Na-poor sample*, includes stars with [Na/Fe]< +0.05 and numbers a total of 288 stars. The second, *Na-rich sample*, is composed of stars with [Na/Fe]> +0.05 for a total of 201 stars. We have checked that the adoption of slightly different boundaries does not affect our results (see Section 4). We verified that the two sub-samples have indistinguishable radial distributions consistent with their parent populations. Based on our present understanding of MP formation, in the following we will sometimes refer to *Na-poor* and *Na-rich* sub-samples as FG and SG stars respectively.

Panel b) of Figure 2 shows the distribution of Na-poor and Na-rich stars in the $(U, U-B)$ CMD (Dalessandro et al. 2014). The two groups appear to be nicely separated on the RGB and in particular, Na-poor stars reside on the bluer side of the RGB (as they are N-poor), while the Na-rich component lies on the red side, as expected (Sbordone et al. 2011).
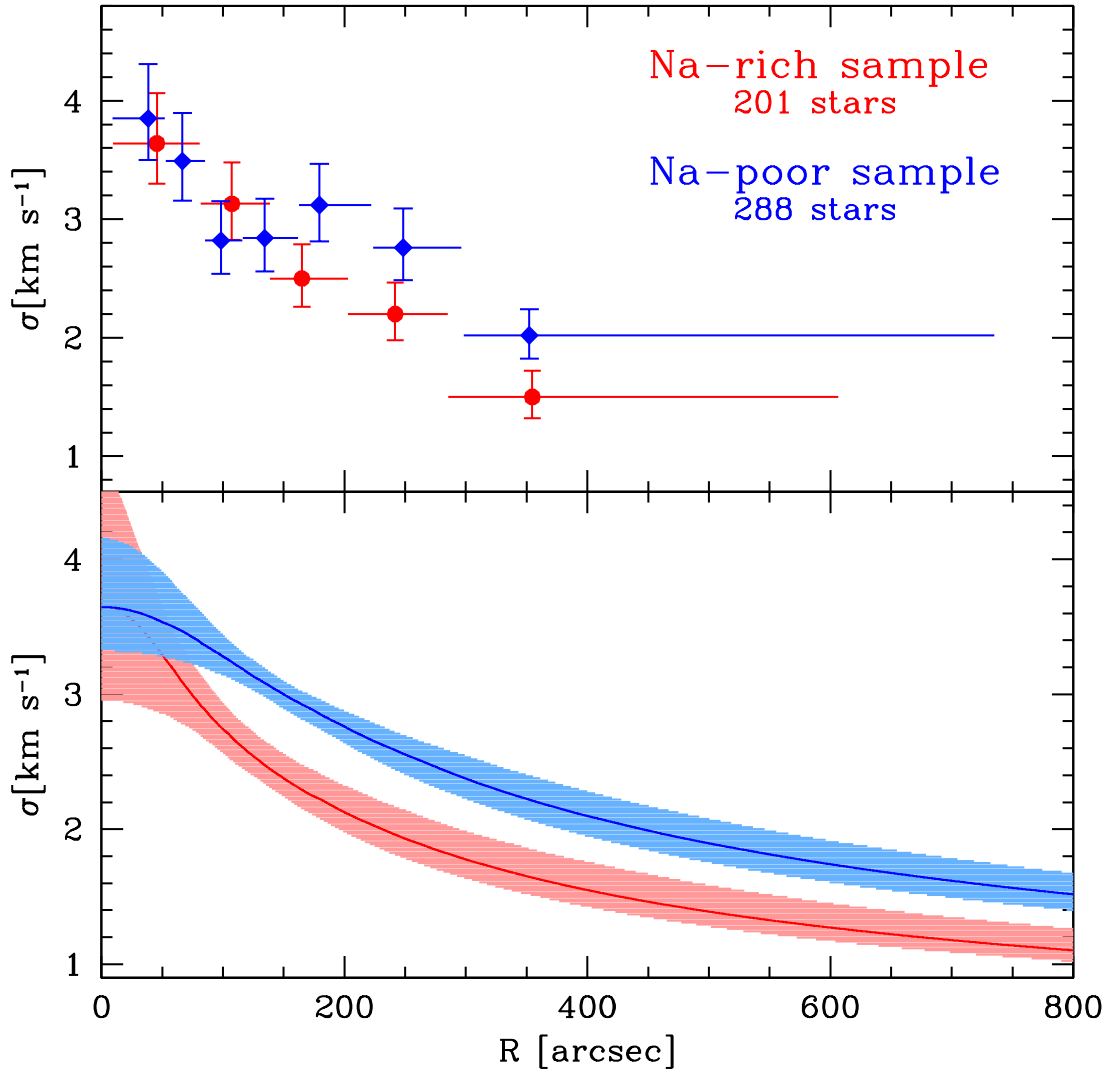
**Figure 3.** Binned velocity dispersion profiles (upper panel) and 1-$\sigma$ confidence regions around the best-fit dispersion profiles (bottom panel) for the *Na-rich* (red) and *Na-poor* (blue) samples.

## 4. KINEMATIC ANALYSIS AND RESULTS

In Figure 3 the line-of-sight velocity dispersion profiles of the two considered sub-samples are compared. In the upper panel we show the binned dispersion profiles for illustration purposes only. They are obtained by assuming an equal number of stars in each bin (apart from the outermost bin which contains any additional leftover stars). We used the Maximum Likelihood estimator of Pryor & Meylan (1993) to compute the velocity dispersion in each bin and its uncertainty. At each bin we assigned the value of the distance corresponding to the mean radius of all the stars in that bin. The corresponding horizontal error bars represent the radial range spanned by the stars in a given bin.

To characterize the kinematics of the *Na-rich* and *Na-poor* samples, we used the maximum likelihood method described in Cordero et al. (2017). We stress that this is a purely kinematic approach aimed at searching for relative differences in the kinematics of sub-populations and not aimed at providing

**Table 1.** Median value and $\pm 1\sigma$ uncertainties (enclosing the central 68% of the probability distribution) obtained from the posterior probability distributions for the free parameters of the different subsamples.

| Sample | $N_{\rm stars}$ | $v_0$ | $\sigma_0$ | $a$ |
|---|---|---|---|---|
| | | [km s$^{-1}$] | [km s$^{-1}$] | [arcmin] |
| Na-poor | 288 | $-14.10^{+0.20}_{-0.19}$ | $3.55^{+0.38}_{-0.28}$ | $2.98^{+1.43}_{-0.96}$ |
| Na-rich | 201 | $-14.61^{+0.22}_{-0.22}$ | $3.61^{+0.60}_{-0.48}$ | $1.69^{+1.11}_{-0.63}$ |
| Total sample | 489 | $-14.33^{+0.14}_{-0.14}$ | $3.61^{+0.32}_{-0.28}$ | $2.13^{+0.76}_{-0.55}$ |

a self-consistent dynamical model of the system. For each sub-sample, we fit a kinematic model to discrete radial velocities. As in Cordero et al. (2017), we assume for the velocity dispersion profile the functional form of the Plummer (1911) model, defined by its central velocity dispersion $\sigma_0$ and its scale radius $a$:

$$\sigma^2(R) = \frac{\sigma_0^2}{\sqrt{1 + R^2/a^2}} \ , \tag{1}$$

where $R$ is the projected distance from the centre of the cluster. Table 1 lists the best-fit values and the uncertainties of the main parameters of our analysis and for the different samples considered.

In the bottom panel of Figure 3 the best-fit Plummer models and the 1-$\sigma$ confidence envelopes on the dispersion profiles are also shown.

A comparison of the velocity dispersion profiles, in particular of those obtained without binning the data clearly shows differences between the velocity dispersion profile of the FG and the SG populations. In particular, while the two profiles are indistinguishable out to about $\sim 70''$-$80''$ (corresponding to $\sim 0.5 \times r_h$ and $\sim 1.5 r_c$; Dalessandro et al. 2014), beyond this radius the SG velocity dispersion profile decreases more sharply than that of the FG and attains values of the dispersion smaller than those of the FG population by $\sim 1$ km s$^{-1}$. This difference represents a large fraction ($\sim 30\%$) of the observed central velocity dispersion values of *Na-poor* and *Na-rich* stars ($\sigma_0 \sim 3.55^{+0.38}_{-0.28}$ km s$^{-1}$ and $\sigma_0 \sim 3.61^{+0.60}_{-0.48}$ km s$^{-1}$ respectively)[2] [3]

*We note that this is the first time that differences in the line-of-sight velocity dispersion of MPs are detected.*

In order to quantitatively assess the significance of this result, we performed a Kolmogorov-Smirnov test on the $RV$s. We find that the probability that the two populations are extracted from the same parent distribution is $P_{\rm KS} \sim 4 \times 10^{-3}$. [4] We have also performed a *F-test* to test the hypothesis that the velocity dispersions of the two samples are equal. We used a maximum-likelihood analysis to derive the intrinsic velocity dispersions for the two sub-samples at different radial distances from

---

[2] On the other hand, we found no significant difference in the overall rotation pattern of the two sub-samples, adopting both the approach of Bellazzini et al. (2012) and that of Cordero et al. (2017). A more detailed analysis of the rotation properties of the cluster will be presented in a companion paper (E. Dalessandro et al. 2018, in preparation).

[3] We point out that we use a Plummer model just as a convenient way of providing a quantitative characterization of kinematical differences; the differences in this kinematical characterization are not meant to have any implication for the spatial distribution of the two populations which as shown in Dalessandro et al. (2014) are spatially mixed.

[4] This test is not directly addressing the significance of the differences between the velocity dispersion profiles, but of the RV distribution. In this respect it important to note that the shape of the cumulative distributions as well as the derived probabilities depend also on the mean velocities of the two samples.

the cluster center. We find that for R> 150″ (which corresponds to the distance where velocity dispersion profiles Na-poor and Na-rich start to differ) the F-test probability is only $\sim 4 \times 10^{-3}$ and it further decreases for R> 200″ ($\sim 4 \times 10^{-3}$). *These results therefore provide strong support to the conclusion that the Na-poor and Na-rich velocity dispersion profiles are significantly different, with Na-poor stars being dynamically hotter.*

Considering the results of our previous study of MPs in NGC 6362 (Dalessandro et al. 2014) showing that the spatial distributions of the FG and SG populations are consistent with being completely mixed, the kinematic difference we have found is surprising. Complete spatial mixing is expected in the advanced stages of a cluster's evolution and after the cluster has undergone significant mass loss. As we will further discuss in Section 6, once a cluster has attained complete spatial mixing, its MPs should also be characterized by similar velocity dispersion profiles. The results found here therefore raises a fundamental question concerning the dynamical ingredients responsible for the observed kinematic differences.

## 5. FG AND SG BINARY FRACTIONS

Before exploring the possible culprit of the observed kinematic differences, we use our radial velocity data to determine the binary fraction in the FG and SG populations. Information about the binary population and the possible differences between the FG and SG binary fractions is extremely important both to build a complete dynamical picture of the cluster and to shed light on the possible role of binaries on the observed kinematic properties presented in the previous section. The finding by Lucatello et al. (2015) that FG stars have typically a larger binary fraction than their SG counterparts seem particularly relevant in this context.

We used a sub-sample of 384 stars observed repeatedly (from a minimum of 2 to a maximum of 6 times; see Section 2) within a period of 704.96 days ($\sim$2 yrs). Candidate binary stars (i.e. those with $\sigma_{RV} > 3$ km s$^{-1}$ – see Section 3) have now been included in the analysis. We stress that this is the largest sample ever used so far for such kind of study for an individual GC.

We followed the approach described in Lucatello et al. (2015) for the binary fraction derivation. For each star in our sub-sample, we performed a $\chi^2$ test by using the single velocities and relative errors to assess whether they are compatible with a non-variable behavior. Stars with $P(\chi^2) < 1\%$ have been flagged as binaries. Among the 384 stars (235 belonging to the FG and 149 to the SG), 12 turned out to be binaries, 11 are FG stars and 1 belong to the SG sub-population. These values correspond to a minimum binary fraction for the entire sample (FG+SG) $f_{min}^{TOT} = 3.1 \pm 0.9\%$, and to $f_{min}^{FG} = 4.7 \pm 1.4\%$ and $f_{min}^{SG} = 0.7 \pm 0.7\%$.

Unfortunately, a significant fraction of binaries cannot be directly detected with our data-set because of their long variability periods and/or not favorable inclination angles. In order to account for these observational limitations and estimate the binary detection efficiency of our observations, we adopted the following approach. For each observed star, we generated a synthetic population of 1000 binaries assuming a primary component mass of 0.85 $M_\odot$ (adequate for a RGB star in NGC 6362), secondary component masses randomly extracted from a flat mass-ratio distribution, periods extracted from a log-normal distribution (using $\langle \log(P/d) \rangle = 4.8$ and $\sigma_{\log(P/d)} = 2.3$; Duquennoy & Mayor 1991), eccentricities extracted using the prescriptions of Duquennoy & Mayor (1991), random inclination angles, periastron longitude and orbital phases. We also forced the binary semi-major axes to lie between the Roche-Lobe overflow distance limit (Lee & Nelson 1988) and that corresponding to the average collisional ionization limit (Hut & Bahcall 1983). The adoption of this additional

criterion reduces the extent of the simulated period distribution to the range $0.4 < \log(P/d) < 5.3$. For each synthetic binary, the luminosity weighted systemic velocities has been computed and it has been sampled with the same cadence as the observations.

Gaussian shifts with standard deviation equal to observational errors have been added to the velocities to mimic the effect of observational uncertainties. As a control population, we also simulated a large number of single stars with constant velocity.

The same analysis performed on the observed sample has been applied to the synthetic populations of binaries and single stars to derive the detection efficiency as a function of period and the false detection frequency. The detection efficiency ranges from $\sim 40\%$ at $\log(P/d)=0.6$ to $\sim 60\%$ at $\log(P/d)=1.6$ with a decreasing tail at large periods reaching zero at $\log(P/d) > 4.5$. Overall, an average detection efficiency of $\sim 26\%$ has been found, while the false detection frequency is $\sim 1\%$. FG stars have a slightly larger detection efficiency with respect to SG ones ($26.7\%$ versus $19.5\%$), likely due to the smaller velocity measurements errors in FG stars characterized by strong Na lines. Based on these results, the global binary fractions of FG and SG turn out to be $f_g^{FG} \sim 14.3\%$ and $f_g^{SG} < 1\%$ respectively.

This analysis, which is based on a sample up to 8 times larger (per individual cluster), confirms previous findings (Lucatello et al. 2015) about the different present-day binary fraction of FG and SG sub-populations. It also provides support to the predictions of the theoretical studies of Vesperini et al. (2011) and Hong et al. (2015, 2016) showing that the SG binary fraction is expected to be smaller than that of the FG population as a result of dynamical evolution.

## 5.1. *The effect of binary fraction differences on the velocity dispersion profiles*

To estimate the potential effect of such different binary fractions on the derived velocity dispersion profiles of FG and SG sub-populations, we first adopted the following approach. Mock observations have been constructed by randomly extracting for each observed star a velocity from a gaussian function with dispersion equal to the line-of-sight velocity dispersion profile at the same cluster-centric distance of the observed star. The same line-of-sight velocity dispersion profile has been adopted for FG and SG stars, following the King (1966) model that best fits the cluster density profile (see Dalessandro et al. 2014). A random number ($rn$) comprised in the range 0-1, extracted from a uniform probability distribution, was assigned to each FG star. For stars with $rn < 0.143$, which corresponds to the estimated global FG binary fraction, a synthetic binary has been simulated with the mass ratios and orbital parameters described above and the corresponding mean velocity shift has been added. The LOS velocity dispersions of the two generations have been then computed using *a)* the entire sample and *b)* only stars with R$> 150''$ (i.e. where the maximum difference has been observed). The same selection criteria adopted for the construction of the observed dispersion profiles and to exclude apparent binaries has been applied in the analysis of the mock observations. A set of 1000 extractions has been performed for both the considered radial ranges and the distribution of differences has been derived. The results are shown in Figure 4. It can be seen that a velocity dispersion difference equal or larger than the observed one can be obtained as a result of the effect of the different binary fractions in $\sim 54\%$ of the simulated cases (if the entire radial range is considered) and in $\sim 28\%$ of the cases when only the outermost radial range is considered. *Hence, the observed difference in the velocity dispersion profile between FG ad SG stars in NGC 6362 is consistent* with being due to the difference in the binary fraction of the two populations.
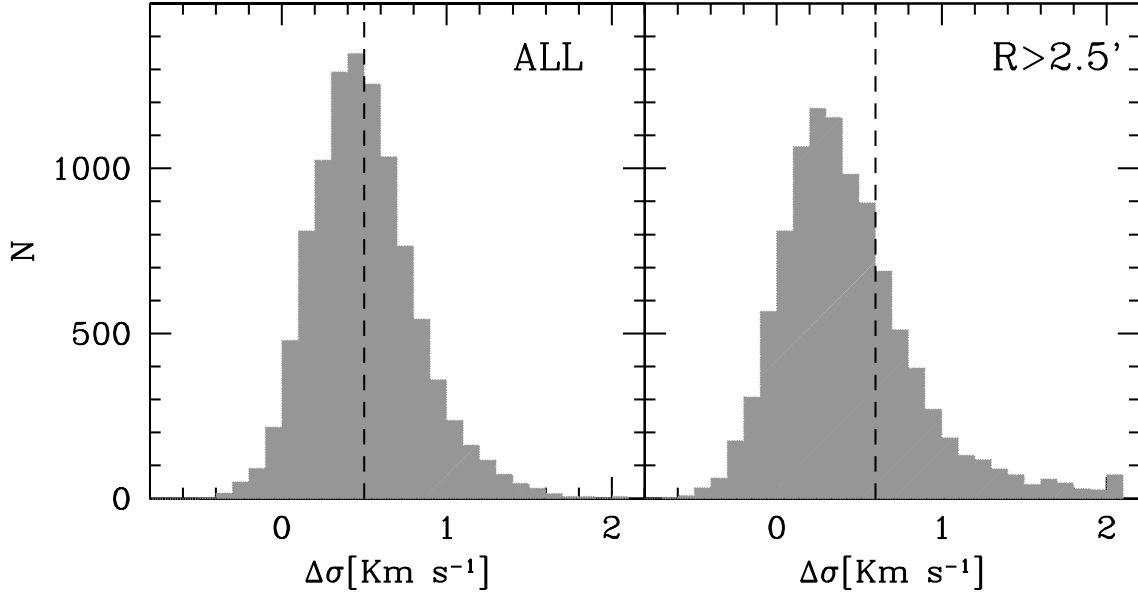
**Figure 4.** Distributions of the velocity dispersion differences obtained as described in Section 4.1 for the entire sample and for stars located at $R > 2.5'$ from the cluster center. Dashed lines represent the observed velocity dispersion differences.

## 6. $N$-BODY MODELS

In order to further explore the possible dynamical history behind the kinematical differences revealed by our observations, we have studied the evolution of the line-of-sight velocity dispersion of FG and SG stars in an $N$-body simulation. The goal here is not to present a model specifically tailored to fit in detail the dynamics of NGC 6362, but rather to gather some fundamental insight on the dynamical ingredients necessary to explain the observational results. For details on the initial conditions of the simulation we refer to Vesperini et al. (2018), here we just summarize the main points. Our simulation starts with a SG population embedded within a more extended FG population: the initial half-mass radius of the FG population is about five times larger than that of the SG population. The simulation starts with 50,000 stars equally split between FG and SG. In this simulation we have focussed our attention on the effects of two-body relaxation on the evolution of the spatial and kinematical properties of the two populations.

In Figure 5 we show the radial profile of the number ratio of SG to FG stars (upper panels) and the ratio profiles of the FG to SG line-of-sight velocity dispersions ($\sigma_{FG}/\sigma_{SG}$; lower panel) representative of two advanced evolutionary stages in our simulation for stars with masses between $0.75 - 0.85 M_\odot$. Although as pointed out above, our analysis is not aimed at providing a detailed fit of the observations, we include in these plots also the observational data from the analysis carried out in this paper and in Dalessandro et al. (2014) to ease a more quantitative comparison between the strength of the observed and theoretical gradients.

The plots of Figure 5 shed light on the close connection between the structural and kinematical properties of the FG and SG populations. For a dynamically old cluster in which the FG and the SG populations are completely spatially mixed (Figure 5 left panels), the $N$-body simulations show that the radial profile of $\sigma_{FG}/\sigma_{SG}$ is flat, at odds with the observations. If we consider a dynamical
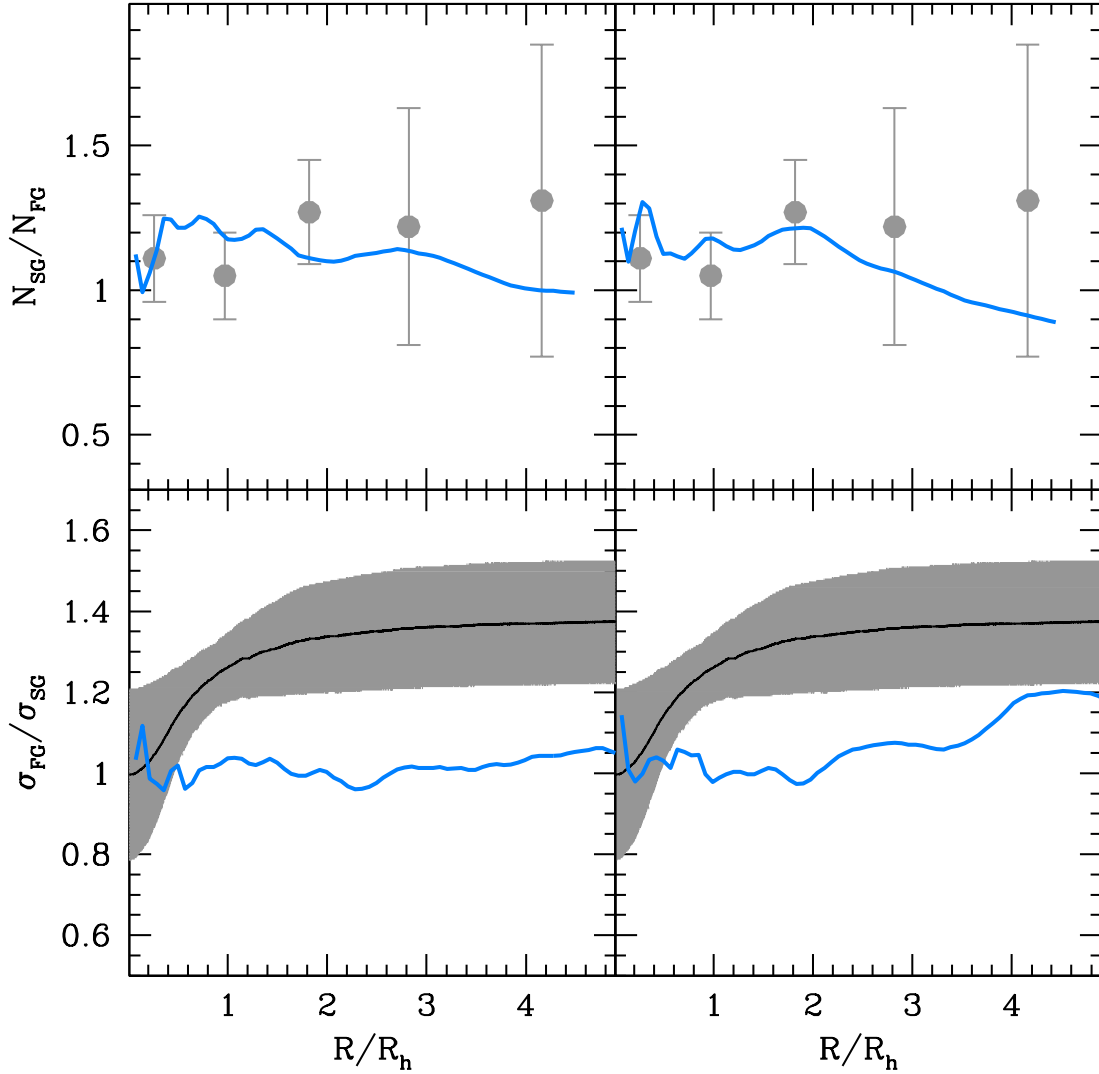
**Figure 5.** *Upper panels*: FG and SG number ratio as a function of the distance from the cluster center normalized to $R_h$ in two advanced snapshots of our $N$-body simulations with no binaries (blue lines). The grey circles represent the number ratio distribution observed in NGC 6362 Dalessandro et al. (2014). *Lower panels*: Radial variations of the ratio of the observed FG to SG line-of-sight velocity dispersions ($\sigma_{FG}/\sigma_{SG}$) from $N$-body models for the same snapshots as before. The dashed grey area represents the observations.

phase characterized by a modest radial gradient in the fraction of SG stars (but still consistent within the errors with the observations; Figure 5 right panels), the $\sigma_{FG}/\sigma_{SG}$ tends to increase in the external regions of the cluster, but the values of $\sigma_{FG}/\sigma_{SG}$ remain smaller than the observed ones at all distances from the cluster center.

Although the discrepancy between the theoretical and the observed radial profile of $\sigma_{FG}/\sigma_{SG}$ can be of the order of $\sim 1.5\sigma$ in the external regions, the systematic underestimate of the ratio compared to the observed one could be an indication that an additional dynamical effect not accounted for in the simulations might be responsible for the observed profile. Indeed, as discussed in Section 5.1, a
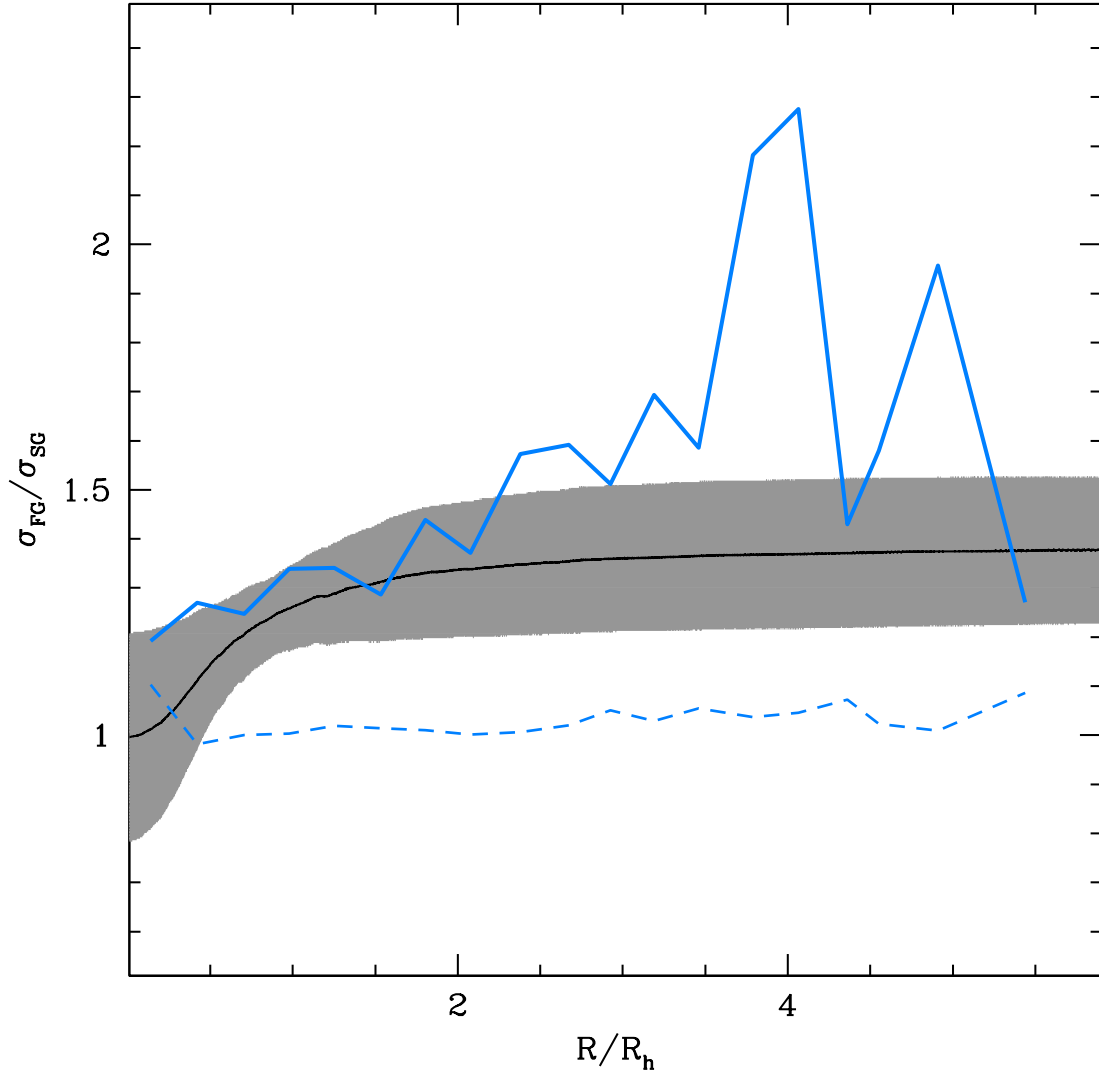
**Figure 6.** Radial variations of the ratio of the observed FG to SG line-of-sight velocity dispersions ($\sigma_{FG}/\sigma_{SG}$) from $N$-body models with binaries (see Section 6) compared to observations (grey dashed area). The dashed line represents the velocity dispersion ratio radial distribution from the same simulation when the effect of binaries is not included.

difference between the FG and SG binary fractions can play a key role in determining the observed differences between the FG and SG velocity dispersion profiles.

As shown in Vesperini et al. (2011) and Hong et al. (2015, 2016), if SG stars form in a more compact and centrally concentrated subsystem than FG stars, as predicted by a number of formation models (see e.g. D'Ercole et al. 2008), all the processes altering the number and orbital properties of binary stars (ionization, hardening, softening, ejection; see e.g. Heggie & Hut 2003) affect the SG binaries more efficiently than the FG ones. One of the consequences of this dynamical difference is the preferential disruption and ejection of SG binaries leading, in turn, to a larger global fraction of FG binaries.

As shown in the study of Hong et al. (2016) and Hong et al. (2018, in preparation), the processes affecting the evolution and survival of binaries have also an effect on their spatial distribution and the spatial mixing of the FG and SG binaries. In particular, the timescale for the spatial mixing of FG and SG binaries can be much longer than that of single stars. This implies that while the FG and SG single stars might have already reached complete spatial mixing, the FG and SG binary populations might still be characterized by a radial gradient, with the fraction of FG to SG binaries increasing as the cluster-centric radius increases (see e.g. bottom panel of Figure 11 in Hong et al. 2016). The difference in the fraction of FG and SG binaries and its radial variation imply that the possible velocity dispersion inflation due to binaries is stronger for the FG population and is increasingly more important at larger distances from the cluster center. As a consequence, differences in the FG and SG binary fraction and in their spatial distribution can contribute to produce a $\sigma_{\mathrm{FG}}/\sigma_{\mathrm{SG}}$ profile increasing with the distance from the cluster center, as found in our observations.

Figure 6 illustrates this effect as measured in one of the simulations (MPr5f1x3-800) presented in Hong et al. (2016). We emphasize that the simulations are still idealized and are not meant to provide a detailed model for NGC 6362 but they include the essential dynamical ingredients necessary to illustrate the effect of interest here. From this analysis and the comparison with the observations it emerges that binaries can play a major role in shaping the $\sigma_{\mathrm{FG}}/\sigma_{\mathrm{SG}}$ radial gradient and could be the dynamical ingredient needed to match the observational results.

Although additional and more realistic simulations are needed to build specific models for NGC 6362, the results presented here clearly illustrate how the study of the kinematics of multiple populations can reveal the fingerprints of a number of fundamental dynamical effects and of their role in shaping the properties of FG and SG stars.

## 7. SUMMARY AND DISCUSSION

The detailed kinematic analysis performed in this work has revealed that Na-poor (FG) and Na-rich (SG) stars are characterized by significantly different line-of-sight velocity dispersion profiles. SG stars have systematically smaller velocity dispersion values than FG ones, with differences of $\sim 1$ km s$^{-1}$ for $R > 70'' - 80''$ (corresponding to $R > 0.5 r_{\mathrm{h}}$). This is the first time that differences in the line-of-sight velocity dispersion of MPs are detected.

Considering that in our previous study on the spatial distribution of MPs in NGC 6362 (Dalessandro et al. 2014) we have found that the FG and SG populations are spatially mixed and that the cluster must be in an advanced stage of its dynamical evolution, the kinematical evidence detected here is surprising and raises a fundamental question concerning the dynamical processes responsible for the difference between the FG and SG velocity dispersion profiles.

Thanks to our large set of RVs we have also been able to estimate the binary fraction in the two populations and found a significant difference between the FG binary fraction ($f \sim 14\%$) and that of the SG population ($< 1\%$). This result is based on the largest sample ever used for this kind of analysis.

By using $N$-body simulations and mock observations, we show that such a large binary fraction difference can play an essential role in determining the observed kinematic differences between the FG and the SG populations found in our study.

Beside the specific case of NGC 6362, the results of this paper clearly demonstrate the importance of the study of the kinematics at several epochs to build a complete dynamical picture of MPs in globular clusters and to shed light on the dynamical history of MPs. In this context it will be

important to extend this kind of analysis to other systems in order to understand whether NGC 6362 is a peculiar case or similar effects are present in all GCs. Moreover, the addition of Gaia proper motions sampling the entire extension of the cluster, will allow us to constrain the degree of anisotropy currently characterizing the system.

More in general, for clusters at different dynamical stages a radial variation of the SG to FG velocity dispersion could be due to a combination of the effect of binaries and a radial gradient in the fraction of SG stars.

Moving a step forward in our comprehension of the kinematics of MPs is, in turn, a key stage in the study of GC formation and evolution.

## REFERENCES

Bastian, N., Lamers, H. J. G. L. M., de Mink, S. E., et al. 2013, MNRAS, 436, 2398

Bastian, N., & Lardo, C. 2017, arXiv:1712.01286

Bekki, K. 2010, ApJL, 724, L99

Bellazzini, M., Bragaglia, A., Carretta, E., et al. 2012, A&A, 538, A18

Bellini, A., Piotto, G., Milone, A. P., et al. 2013, ApJ, 765, 32

Bellini, A., Vesperini, E., Piotto, G., et al. 2015, ApJL, 810, L13

Bragaglia, A., Carretta, E., D'Orazi, V., et al. 2017, arXiv:1708.07705

Carney, B. W., Latham, D. W., Stefanik, R. P., Laird, J. B., & Morse, J. A. 2003, AJ, 125, 293

Chung, C., Yoon, S.-J., & Lee, Y.-W. 2011, ApJL, 740, L45

Conroy, C. 2012, ApJ, 758, 21

Cordero, M. J., Hénault-Brunet, V., Pilachowski, C. A., et al. 2017, MNRAS, 465, 3515

Dalessandro, E., Massari, D., Bellazzini, M., Miocchi, P., Mucciarelli, A., Salaris, M., Cassisi, S., Ferraro, F. R., & Lanzoni, B., 2014, ApJ, 791L, 4

Dalessandro, E., Lapenna, E., Mucciarelli, A., et al. 2016, ApJ, 829, 77

Decressin, T., Meynet, G., Charbonnel, C., Prantzos, N., & Ekström, S. 2007, A&A, 464, 1029

Decressin, T., Baumgardt, H., & Kroupa, P. 2008, A&A, 492, 101

de Mink, S. E., Pols, O. R., Langer, N., & Izzard, R. G. 2009, A&A, 507, L1

Denissenkov, P. A., & Hartwick, F. D. A. 2014, MNRAS, 437, 21

D'Ercole, A., Vesperini, E., D'Antona, F., McMillan, S. L. W., & Recchi, S. 2008, MNRAS, 391, 825

D'Ercole, A., D'Antona, F., Ventura, P., Vesperini, E., & McMillan, S. L. W. 2010, MNRAS, 407, 854

Duquennoy, A., & Mayor, M. 1991, A&A, 248, 485

Foreman-Mackey, D., Hogg, D. W., Lang, D., & Goodman, J. 2013, PASP, 125, 306

Gratton, R. G., Carretta, E., & Bragaglia, A. 2012, A&A Rv, 20, 50

Heggie, D., & Hut, P. 2003, The Gravitational Million-Body Problem: A Multidisciplinary Approach to Star Cluster Dynamics, by Douglas Heggie and Piet Hut. Cambridge University Press, 2003, 372 pp.,

Hénault-Brunet, V., Gieles, M., Agertz, O., & Read, J. I. 2015, MNRAS, 450, 1164

Hong, J., Vesperini, E., Sollima, A., et al. 2016, MNRAS, 457, 4507

Hong, J., Vesperini, E., Sollima, A., et al. 2015, MNRAS, 449, 629

Hut, P., & Bahcall, J. N. 1983, ApJ, 268, 319

King, I. R. 1966, AJ, 71, 64

Kirby, E. N., Simon, J. D., & Cohen, J. G. 2015, ApJ, 810, 56

Lardo, C., Bellazzini, M., Pancino, E., et al. 2011, A&A, 525, A114

Larsen, S. S., Brodie, J. P., Grundahl, F., & Strader, J. 2014, ApJ, 797, 15

Larsen, S. S., Baumgardt, H., Bastian, N., et al. 2015, ApJ, 804, 71

Lee, H. M., & Nelson, L. A. 1988, ApJ, 334, 688

Lind, K., Asplund, M., Barklem, P. S., & Belyaev, A. K., 2011, A&A, 528, 103

Lucatello, S., Sollima, A., Gratton, R., et al. 2015, A&A, 584, A52

Martocchia, S., Cabrera-Ziri, I., Lardo, C., et al. 2017, arXiv:1710.00831

Massari, D., Lapenna, E., Bragaglia, A., et al. 2016, MNRAS, 458, 4162

Massari, D., Mucciarelli, A., Dalessandro, E., Bellazzini, M., Cassisi, S., Fiorentino, G., Ibata, R. A., Lardo, C., Salaris, M., 2017, MNRAS, 468, 1249

Mastrobuono-Battisti, A., & Perets, H. B. 2013, ApJ, 779, 85

Merritt, D., Meylan, G., & Mayor, M. 1997, AJ, 114, 1074

Meylan, G., & Mayor, M. 1986, A&A, 166, 122

Miholics, M., Webb, J. J., & Sills, A. 2015, MNRAS, 454, 2166

Milone, A. P., Piotto, G., Bedin, L. R., et al. 2012, ApJ, 744, 58

Mucciarelli, A., Origlia, L., Ferraro, F. R., & Pancino, E., 2009, ApJ, 659L, 134

Mucciarelli, A., Bellazzini, M., Ibata, R., et al. 2012, MNRAS, 426, 2889

Mucciarelli, A., Pancino, E., Lovisi, L., Ferraro, F. R., & Lapenna, E., 2013, ApJ, 766, 78

Mucciarelli, A., Bellazzini, M., Catelan, M., Dalessandro, E., Amigo, P., Correnti, M., Cortes, C., & D'Orazi, V., 2013, MNRAS, 435, 3667

Mucciarelli, A., Dalessandro, E., Massari, D., Bellazzini, M., Ferraro, F. R., Lanzoni, B., Lardo, C., Salaris, M., & Cassisi, S., 2016, ApJ, 824, 73

Muratov, A. L., & Gnedin, O. Y. 2010, ApJ, 718, 1266

Pasquini, L., et al., 2000, SPIE, 4008, 129

Piotto, G., Milone, A. P., Bedin, L. R., et al. 2015, AJ, 149, 91

Plummer, H. C. 1911, MNRAS, 71, 460

Pryor, C., & Meylan, G. 1993, Structure and Dynamics of Globular Clusters, 50, 357

Sbordone, L., Salaris, M., Weiss, A., & Cassisi, S. 2011, A&A, 534, A9

Richer, H. B., Heyl, J., Anderson, J., et al. 2013, ApJL, 771, L15

Savino, A., Massari, D., Bragaglia, A., Dalessandro, E., & Tolstoy, E. 2018, MNRAS, 474, 4438

Schiavon, R. P., Caldwell, N., Conroy, C., et al. 2013, ApJL, 776, L7

Simioni, M., Milone, A. P., Bedin, L. R., et al. 2016, MNRAS, 463, 449

Stetson, P. B., & Pancino, E., 2008, PASP, 120, 1332

Tiongco, M. A., Vesperini, E., & Varri, A. L. 2017, arXiv:1704.05918

van de Ven, G., van den Bosch, R. C. E., Verolme, E. K., & de Zeeuw, P. T. 2006, A&A, 445, 513

Vesperini, E., McMillan, S. L. W., D'Antona, F., & D'Ercole, A. 2011, MNRAS, 416, 355

Vesperini, E., McMillan, S. L. W., D'Antona, F., & D'Ercole, A. 2013, MNRAS, 429, 1913

Vesperini, E., Hong, J., Webb, J. J., D'Antona, F., & D'Ercole, A. 2018, MNRAS, 476, 2731

Watkins, L. L., van der Marel, R. P., Bellini, A., & Anderson, J. 2015, ApJ, 803, 29